Effect of D To E mutation of the RGD motif in rhodostomin on its activity, structure, and dynamics: Importance of the interactions between the D residue and integrin

Chiu-Yueh Chen,[1,2] Jia-Hau Shiu,[1,2] Yao-Husn Hsieh,[1,2] Yu-Chen Liu,[1,2] Yen-Chin Chen,[1,2] Yi-Chun Chen,[1,2] Wen-Yih Jeng,[1,2] Ming-Jer Tang,[3] Szecheng J. Lo,[4] and Woei-Jer Chuang[1,2]*

[1] Department of Biochemistry, National Cheng Kung University College of Medicine, Tainan 701, Taiwan

[2] Institute of Basic Medical Sciences, National Cheng Kung University College of Medicine, Tainan 701, Taiwan

[3] Department of Physiology, National Cheng Kung University Medical College, Tainan 701, Taiwan

[4] Department of Life Science, Chang-Gung University, Tao-Yuan, 333, Taiwan

ABSTRACT

Rhodostomin (Rho) is a snake venom protein containing an RGD motif that specifically inhibits the integrin-binding function. Rho produced in *Pichia pastoris* inhibits platelet aggregation with a K_I of 78 nM as potent as native Rho. In contrast, its D51E mutant inhibits platelet aggregation with a K_I of 49 μM. Structural analysis of Rho and its D51E mutant showed that they have the same tertiary fold with three two-stranded antiparallel β-sheets. There are no structural backbone differences between the RG[D/E] loop which extends outward from the protein core and the RG[D/E] sequence at its apex in a four-residue RG[D/E]M type I turn. Two minor differences between Rho and its D51E mutant were only found from their backbone dynamics and 3D structures. The R_2 value of E51 is 13% higher than that of the D51 residue. A difference in the charge separation of 1.76 Å was found between the sidechains of positive (R49) and negative residues (D51 or E51).The docking of Rho into integrin $\alpha v\beta 3$ showed that the backbone amide and carbonyl groups of the D51 residue of Rho were formed hydrogen bonds with the integrin residues R216 and R214, respectively. In contrast, these hydrogen bonds were absent in the D51E mutant-integrin complex. Our findings suggest that the interactions between both the sidechain and backbone of the D residue of RGD-containing ligands and integrin are important for their binding.

Proteins 2009; 76:808–821.
© 2009 Wiley-Liss, Inc.

Key words: disintegrin; dynamics; *Pichia pastoris*; RGD motif; rhodostomin; structure.

INTRODUCTION

The tripeptide sequence Arg-Gly-Asp (RGD) is the consensus sequence of many adhesive proteins such as fibronectin, fibrinogen, vitronectin, and von Willebrand factor.[1] In mammals, 18 α and 8 β subunits assemble into 24 integrins that have different specificity and affinity for their ligand binding.[2–5] The RGD sequence is recognized by half of the 24 known integrins, whereas alternative short peptide sequences are recognized by other integrins.[6] In addition to extracellular matrix proteins, the RGD sequence is found in many proteins, including dendroaspin, decorsin, savignygrin, streptopain, γ-bungarotoxin, human herpesvirus eight envelope glycoprotein B, and disintegrins.[7–12] Disintegrins are the peptides found in snake venoms of the viper family and mainly inhibit the functions of β1- and β3-associated integrins.[12] They were first identified as inhibitors of platelet aggregation and were subsequently shown to bind with high affinity to integrins and to block the interaction of integrins with RGD-containing proteins. They contain 47 to 84 amino acids with from 4 to 7 disulfide bonds.[12–14] The conserved RGD or KGD sequences in this disintegrin family play the most important role in recognizing the integrin $\alpha_{IIb}\beta_3$.[12,13] Many 3D structures of disintegrins, including kistrin (Rhodostomin and kistrin are synonymous), echistatin, flavoridin, albolabrin, trimestatin, and salmosin, were determined using NMR spectroscopy and X-ray crystallography.[15–20] Analyses of these structures showed that they consist of a series of

tightly packed loops and turns held together by disulfide bonds. The RGD motif, the important binding site for integrin, lies in a mobile loop ranging from 5 to 11 residues joining two strands of β sheet. The RGD sequence is located at the apex of a long loop, between two β strands of the protein, protruding 10–17 Å from the protein core.[13] The R and D sidechains in the loop do not interact but nearly oppose each other by 180°.

Many studies have shown that alternations in the residues in or flanking the RGD motif of RGD-containing proteins affect their binding specificities and affinities for integrins.[7,10,21,22] Specifically, the residues in the RGD motif of RGD-containing proteins play the most important role in interacting with integrins.[5,23] The mutation of D to E in kistrin causes a greater than 100-fold decrease in activity.[23] Site-directed mutagenesis of D to E in the RGD motif of vitronectin abolishes cell adhesion.[24] The importance of the D residue has been observed in peptides as well. For example, RGD-containing peptide YGRG**D**SP inhibits integrin function. In contrast, its mutant YGR-G**E**SP, containing a conservative D to E mutation, does not interact with integrins.[25] These studies indicate that the conserved D residue of the RGD motif is most critical residue for the interaction of RGD ligand with integrins. However, little is known about how a conservative D to E mutation on the RGD motif of RGD-containing proteins causes a significant effect on its activity.

In the present study, we used rhodostomin as the model protein to study the effect of the mutation of D to E on dynamics and structure-activity relationships of RGD-containing proteins. Rho is obtained from *Callose-lasma rhodostoma* venom and belongs to the family of disintegrins.[26,27] It consists of 68 amino acids, including 12 residues of cysteine and an RGDMP sequence at positions of 49–53. We previously showed that Rho expressed in *P. pastoris* possesses the same function and structure as native protein.[27,28] Therefore, we expressed D51E mutant of Rho in *P. pastoris*, determined its activity in the inhibition of platelet aggregation, and used nuclear magnetic resonance (NMR) spectroscopy to compare the structural and dynamic differences between Rho and its D51E mutant. We also docked Rho and its D51E mutant into integrin αvβ3 and analyzed their interactions. The results from our functional, structural, and dynamic studies revealed that the interactions between integrin and both the sidechain and backbone of the D residue in the RGD motif of RGD-containing proteins are important in integrin binding.

METHODS

Expression of Rho and its D51E mutant in *P. pastoris* and purification

The expression of Rhodostomin and its D51E mutant in *P. pastoris* was accomplished by following protocols previously described.[27] The wild-type construct was used to produce D51E mutation using overlap extension PCR.[29] The expression kit and the yeast transfer vector, pPICZαA, were purchased from Invitrogen. The structural gene of *Rho* was amplified using polymerase chain reaction (PCR) with sense primer 5′-GAATTCGAATTC CATCA TCATCATCATCATGGTAAGGAATGTGACTGTT CTT-3′ that has *EcoR1* recognition and six histidine residues for facilitating purification. The antisense primer was 5′-CCGCGG CCGCGGTTAGTGGTATCTTGGAC AGTCAGC-3′ with *Sac* II recognition and TTA stop codon. The PCR product was purified and then cloned into the *EcoR1* and *Sac* II sites of yeast recombination vector, pPICZαA. The recombinant plasmid was transformed into *DH5α* strain, and the colony was selected by agar plate with low salt LB (1% tryptone, 0.5% yeast extract, 0.5% NaCl, and 1.5% agar at pH 7.0) and 25 μg/mL of the antibiotic Zeocin. After the clone had been confirmed by sequencing the insert, 10 μg of plasmid was digested with *Sac* I to linearize the plasmid. The linearized construct was transformed into the *Pichia* strain X33 using a kit (*Pichia* EasyComp; Invitrogen). The transformant integrated at the 5′ AOX1 locus with a single crossover, and the colony was selected by agar plate using YPDS (1% yeast extract, 2% peptone, 2% glucose, 2% agar, and 1 M Sorbitol) and 100 μg/mL of Zeocin. PCR analysis was used to analyze *Pichia* integrants to determine whether the gene had integrated into the *Pichia* genome. From a number of clones with multiple copies of gene insertion, we chose the clone with the highest protein expression.

Unlabelled Rho and its D51E mutant were produced as follows: 100 μL of cell stock was grown at 30°C for 48 h in 200 mL of yeast extract peptone dextrose (YPD) medium (1% yeast extract, 2% peptone, and 2% dextrose) and 100 μg/mL Zeocin. Cells were then transferred into 800 mL of YPD medium. After another 48 h, the cells were collected by centrifugation and grown in 1 L of minimal methanol medium (1.34% yeast nitrogen base (YNB) with ammonium sulfate without amino acids, 4×10^{-5}% biotin, and 1% Methanol). Once every 24 h, 1% methanol was added to induce protein expression for 2 days. ^{15}N-labelled Rho and D51E mutant were produced as follows: 100 μL of cell stock was grown at 30°C for 48 h in 200 mL of ^{15}N minimal medium (0.34% YNB without ammonium sulfate and amino acids, 2% dextrose, 4×10^{-5}% biotin, and 0.05% [15]NH$_4$Cl) in 100 mM potassium phosphate buffer at pH 6 with 100 μg/mL Zeocin. The cells were then transferred into 800 mL of ^{15}N minimal medium. After another 48 h, the cells were collected by centrifugation and grown in 1 L of ^{15}N minimal methanol medium (0.34% YNB without ammonium sulfate and amino acids, 4×10^{-5}% biotin, 1% Methanol, and 0.05% [15]NH$_4$Cl). Once every 24 h, 1% methanol was added to induce protein expression for 2 days. The supernatant was collected by centrifugation

and dialyzed twice against 5 L of H_2O and once against 5 L of 20 mM Tris-HCl and 200 mM NaCl at pH 8. The final solution was loaded into a nickel-chelating column and eluted with a gradient of 200 mM imidazole. The recombinant Rho proteins produced in *P. pastoris* were further purified by reverse-phase C18 HPLC with a gradient of 15% to 18% acetonitrile. A tricine-SDS-PAGE analysis confirmed that the purification of proteins was greater than 95%.[30]

Mass spectrometric measurements

The molecular weights of proteins were confirmed using an API 365 triple quadrupole mass spectrometer equipped with a TurboIonSpray source (PE Sciex, Thornill, Canada). The protein solutions (1–10 μM in 50–90% methanol or acetonitrile with 0.1% formic acid) were infused into the mass spectrometer using a syringe pump (Harvard Apparatus, South Natick, MA, USA) at a flow rate of 12–20 μL/min to acquire full scan mass spectra. The electrospray voltage at the spraying needle was optimized at 5000–5300 V. The molecular weights of proteins were calculated by computer software provided with the API 365 mass spectrometer.

Platelet aggregation assay

Venous blood (9 parts) from healthy donors who had not received any medication for at least 2 weeks was collected in 3.8% sodium citrate (1 part). Blood was centrifuged at 70g for 10 min to obtain platelet-rich plasma (PRP) and allowed to stand for 5 min. Then, PRP was collected. Platelet-poor plasma (PPP) was prepared from the remaining blood by centrifuging at 800g for 10 min. PPP platelet count was measured on a hematology analyzer and diluted to 250,000 platelets/μL. A solution of 190 μL of PRP and 10 μL of either Rho or PBS buffer was incubated for 5 min in aggregometer (Hema Tracer 601; Niko Bioscience, Inc, Tokyo, Japan) at 37°C. Ten microliters of 200 mM ADP was added to monitor the response of platelet aggregation by light transmission.

NMR spectroscopy

NMR experiments were performed at 27°C on a Bruker Avance 600 spectrometer equipped with pulse field gradients and xyz-gradient triple-resonance probes. In NMR experiments, samples were dissolved in 10% D_2O/90% H_2O or 100% D_2O at a concentration of 2.0 mM; pH was adjusted to 2.0, 4.0, 6.0, or 6.5 using 100 mM KOD. The data were processed on the SGI O_2 or Indigo 2 Extreme using the XWINNMR software and analyzed using the Aurelia software. 2D NOESY, TOCSY, and DQF-COSY NMR spectra were recorded in the phase-sensitive absorption mode with quadrature detection in both F1 and F2 dimensions.[31] A concentration of 3 mM ^{15}N labeled Rho was used to perform 2D ^{1}H-^{15}N

HSQC, 3D ^{1}H-^{15}N edited-TOCSY- and NOESY-HSQC experiments.[32] Mixing times of 30-90 and 60-150 ms were used for TOCSY and NOESY experiments, respectively. The center frequencies of double resonance experiments were 4.75 ppm (^{1}H) and 118 ppm (^{15}N). The observed ^{1}H chemical shifts were referenced with respect to H_2O or HOD signal, which was taken as 4.754 ppm downfield from external sodium 3-trimethylsilylpropionate-2,2,3,3-d4 (TSP) in D_2O (0.0 ppm) at 300 K. The nitrogen chemical shift was referenced to external ^{15}NH$_4$Cl (3 mM in 1M HCl) at 300 K, which is 24.93 ppm downfield from liquid NH_3.

Structure calculations

Structures were calculated using the X-PLOR program with the hybrid distance geometry-dynamical simulated annealing method.[33,34] NOESY cross-peak intensities were categorized into strong, medium, weak, and very weak, which were converted into distance constraints of 1.8–2.8, 1.8–3.6, 1.8–5.0, and 2.5–6.0 Å, respectively. Pseudoatom corrections were used for methylene, methyl, and aromatic protons, and an additional 0.5 Å was added to the upper limit distances involving methyl protons. The dihedral angles ϕ were determined from the ^{3}J$_{NH\alpha}$ coupling constants. For ^{3}J$_{NH\alpha}$ values less than 5 Hz, ϕ values were restricted from $-25°$ to $-95°$, and for ^{3}J$_{NH\alpha}$ values greater than 9 Hz, ϕ values were restricted from $-100°$ to $-170°$. Backbone hydrogen bonds within the antiparallel β-sheets were identified according to the criteria previously laid out.[35] Two restraints were used for each NH-CO backbone hydrogen bond with d $_{N-O}$ restricted to 2.4–3.3 Å and d $_{H-O}$ to 1.7–2.3 Å. A family of 200 structures was generated using NOE distance, dihedral angle, and hydrogen bond restraints. The S-S covalent bonds were deleted and reintroduced as pseudo-NOE distances with the S-S distances constrained to the upper limit of 2.1 Å. During the first phase of dynamics at 2000 K, the value of the force constant of the NOE term was kept constant at 50 kcal mol^{-1} Å^{-2}. The repulsion term was gradually increased from 0.03 to 4.0 kcal mol^{-1} Å^{-2}, and the torsion angle term from 5 to 200 kcal mol^{-1} rad^{-2}. The simulated annealing refinement consisted of a 9-ps cooling dynamics and then 200 cycles of Powell minimization. The twenty lowest-energy structures were accepted based on violations of distance restraints less than 0.5 Å, dihedral angle restraints less than 5°, a van der Waals energy cut-off value of 35 kcal/mol, and an NOE energy cut-off value of 55 kcal/mol. The structure figures were prepared using the MOLMOL program.[36]

Measurements of NMR dynamics

Backbone dynamics of Rho and its D51E mutant were studied by two-dimensional proton-detected het-

eronuclear nuclear magnetic resonance spectroscopy. The ^{15}N- spin-lattice (R_1) and spin-spin (R_2) relaxation rate constants and steady-state ^1H-^{15}N NOEs were measured from ^1H-detected ^1H-^{15}N correlation spectra recorded with sensitivity-enhanced pulse sequences.[37] A series of 10 experiments with relaxation delays of 20, 100, 250, 400, 500, 600, 800, 1000, 1500, and 3000 ms were carried out to measure T_1. A series of 10 experiments with relaxation delays of 30, 50, 70, 90, 110, 150, 200, 300, 500, and 1000 ms were carried out to measure T_2. The longitudinal and transverse relaxation rate constants, R_1 and R_2, were obtained from exponential fits of the peak height data using least-squares fit software SigmaPlot (Jandel Scientific Software, San Rafael, CA, USA). The reported R_i values are the mean values of two independent data sets. In NOE experiment, two spectra one with the NOE and one without were collected. A recycle delay of 6 s was used, and 256 complex t_1 increments of 32 scans were acquired. The NOE effect was calculated as the ratio of peak heights in spectra collected with and without NOE. The reported NOE value was the average value from three pairs of NOE experiments.

The heteronuclear ^{15}N relaxation rate constants, R_1 and R_2, and the ^1H-^{15}N steady state NOE values were analyzed using the FastModelFree program.[38] This program is based on the model-free formalism that was pioneered by Lipari and Szabo.[39] In this approach, the overall and internal molecular motions were assumed to be independent, and the spectral density function for a molecule undergoing isotropic tumbling was calculated using the appropriate expression,

$$J(\omega) = 2/5[(S^2\tau_m/[1 + (\omega\tau_m)^2]) + (S_f^2 - S^2\tau/[1 + (\omega\tau)^2])]$$

where $1/\tau = 1/\tau_m + 1/\tau_e$ and $S^2 = S_s^2 S_f^2$, τ_m is overall rotational correlation time of the molecule, τ_e is the effective correlation time for the motions on the slower of the two time scale, S^2 is the square of the generalized order parameter, and S_s^2 and S_f^2 are the squares of order parameters for the motion on the fast and slow time scale, respectively.[39,40] The axially symmetric diffusion tensor was employed and the atomic coordinates were obtained from the PDB files 2PJF and 2PJG. The program QUADRIC DIFFUSION was used to calculate the diffusion tenors of Rho and its D51E mutant for axially-symmetric motional models from experimental ^{15}N spin relaxation data.[41] The dynamic model describing internal motion was selected in a residue-specific manner, and the numerical optimization procedure described by Mandel *et al.* was used to estimate the involved parameters for a model.[40] All optimization procedures were involved in minimization of the χ^2 function.[40]

Molecular docking

The docking of Rho and its D51E mutant to integrin αvβ3 was performed with the docking program HAD-DOCK Version 1.3 using hydrogen bond and distance restraints.[42] The starting structures for the docking were the average minimized NMR structures of Rho and integrin αvβ3 (PDB code 1L5G).[43] The interaction restraints were derived from X-ray structure of integrin αvβ3 in complex with a cyclic pentapeptide (c(-RGDf[NMe]V-)) using the software iMoltalk.[44] The defined distance threshold was 4 Å, and the interaction restraints between the RGD motif and integrin were used for calculation. The input restraints between the R49, G50, and D51/E51 residues and integrin αvβ3 were 34, 10, and 40, respectively. They were the contacts between the R49 residue and the residues Asp150, Tyr178, Gln180 and Asp218 of integrin αv, between the G50 residue and the residues R216 and A218 of β3, and between the D51/E51 residue and the residues Ser121, Tyr122, Ser123, Arg214, Asn215, Arg216, Asp217, and Ala218 and Mn^{2+} of the MIDAS of β3. Additional 0.5 Å distance was added to the upper and lower limit in interaction restraints. Using these restraints, the standard HAD-DOCK protocol for protein docking was performed with minor modifications. This protocol combines three stages of molecular dynamics calculations, including heating and cooling with a progressive increase of the flexibility at the binding interface. In a first stage, 500 conformations were calculated using a rigid-body docking protocol. The best 100 structures in terms of their intermolecular energies were refined by semiflexible simulated annealing in the second stage. Both the side-chains and the backbone atoms of the residues 46–54 of Rho, 149–152, 176–181, 211–216, and 217–219 of αv, 120–124 and 212–221 of β3 were defined flexible and allowed them to move in a semi-rigid-body docking protocol to search for conformational rearrangements. The resulting 100 structures with the lowest intermolecular energy values were refined with explicit water molecules in the last stage. The structures were classified by clustering based on the pairwise RMSD differences. Two clusters of structures were found by fitting them over the RGD residues with an average RMSD value <1.5 Å for the backbone atoms of all the amino acids in 100 integrin complexes.

Protein data bank accession number and NMR assignment

The coordinates of 20 calculated structures of Rho and its D51E mutant have been deposited in the Protein Data Bank under accession numbers 2PJF and 2PJG, respectively. ^1H and ^{15}N resonances of Rho have been deposited in the BioMagResBank databank under accession number BMRB-5117.

RESULTS

Protein expression and purification of Rho and its D51E mutant

Rho and its D51E mutants were expressed with pPICZαA vector in X33 *P. pastoris*. Rho and its D51E mutant produced in *P. pastoris* were purified to homogeneity by Ni^{2+}-chelating chromatography and C18 reversed-phase HPLC. According to SDS-polyacrylamide gel electrophoresis (data not shown), Rho and D51E mutant produced in *P. pastoris* were homogenous. The yields of Rho and its D51E mutant produced in *P. pastoris* were 10–20 mg/L. Mass spectrometry was used to determine their molecular weights. The experimental molecular weights of Rho and D51E mutant produced in *P. pastoris* were 8416.8 ± 1 and 8431.1 ± 1, in excellent agreement with the calculated values of 8417.3 and 8431.3. These values were calculated by assuming all cysteines formed disulfide bonds, which indicated the formation of six disulfide bonds in Rho and its D51E mutant.

Inhibition of platelet aggregation

Rho produced in *P. pastoris* inhibited platelet aggregation with a K_I of 78.2 ± 6.5 n*M*, as potent as native Rho.[26] In contrast, its D51E mutant inhibited platelet aggregation with a K_I of 49.1 ± 22.2 µ*M*. The mutation of D to E in Rho caused a 628-fold decrease in activity in the inhibition of platelet aggregation. These results demonstrate that the D51 residue in the RGD motif of Rho plays the most important role in the interaction between Rho and integrin αIIbβ3 of platelets.

Structure determination

The solution structures of Rho and its D51E mutant expressed in *P. pastoris* were determined by NMR spectroscopy and the hybrid distance geometry-dynamical simulated annealing method. NMR spectra were recorded at pH 2, 4, 6, and 6.5. Upon raising the pH from 6 to 6.5, many of the amide proton resonances decreased in intensity. Therefore, NMR spectra at pH 6 were chosen for structure determination. NMR assignments of Rho and its D51E mutant were obtained by analyzing standard 2D homonuclear and 3D heteronuclear NMR data. We also performed NOESY experiments using Rho and its D51E mutant at pH 2, 4, and 6 in 100% D_2O to determine their six disulfide bonds. Their pairings were determined by searching CβH to CβH, CαH to CβH, and CαH to CαH NOEs between different cysteines. All six cysteine pairs (C4–C19, C6–C14, C13–C36, C27–C33, C32–C57, and C45–C64) of Rho and its D51E mutant were found from their NOE patterns in the spectra (data not shown). They were consistent with the reported assignments of cysteine pairs for native Rho.[27,28] The secondary structures of Rho and its D51E mutant consisted of seven turns (residues 8–11, 11–14, 22–

25, 34–37, 40–43, 49–52, and 58–61) and three short regions of two-stranded antiparallel β-sheets (residues 14–16 and 22–19, 32–34 and 37–39, and 43–45 and 55–57). The formations of three two-stranded antiparallel β-sheets were characterized by the CαH-CαH, CαH-NH, and NH-NH NOE patterns of the connecting strands, the slowly exchanging amide protons, and the downfield-shifted α protons.

NMR analyses of Rho and its D51E mutant demonstrated that they have the same secondary structures and tertiary fold (see Fig. 1). The superimposition of the ^{15}N-HSQC spectra of Rho and its D51E mutant is shown in Figure 1. The chemical difference was calculated using the formula: $\Delta\delta = ((0.2\Delta\delta_N)^2 + (\Delta\delta_H)^2)^{1/2}$. We did not observe a large number of chemical shift differences between Rho and its D51E mutant. Chemical shift differences larger than 0.1 ppm were observed only for the residues close to the site of mutation, including G50, D51/E51, and M52, which were 0.15, 0.20, and 0.37 ppm, respectively. Rho and its D51E mutant have similar NOE patterns (Supporting Information Figures S1 and S2). All the sequential NOEs of aliphatic protons to NH were observed. Only NOE between D51Hβ and M52NH in Rho, as well as NOEs between E51Hβ and M52NH and E51Hγ and M52NH in Rho D51E mutant were found (Supporting Information Figure S1). Similarly, only NOE between D51Hβ and D51Hα in Rho, as well as NOEs between E51Hβ and
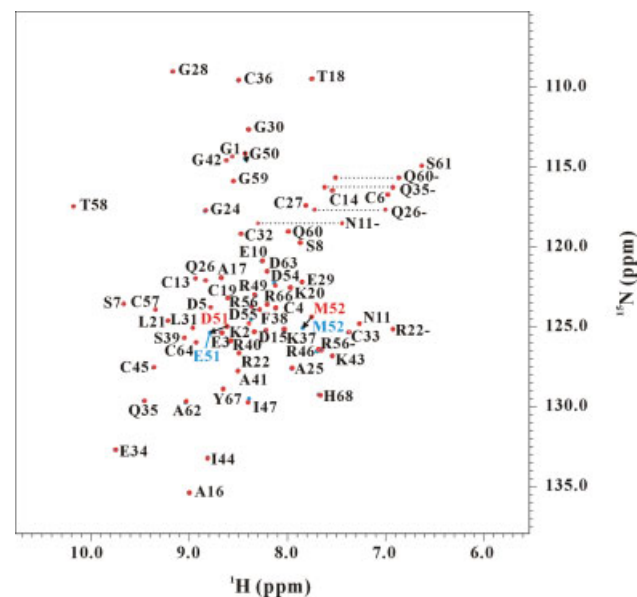
Figure 1

2D ^1H-^{15}N HSQC spectra of Rho (red) and its D51E mutant (blue) at pH 6. Correlation peaks are labeled according to residues type and sequence number. The peaks connected by dotted lines correspond to Gln and Asn side chain NH_2 group. In addition, the resonances of the side chains were labeled with the − sign. The residues G50, D51/E51, and M52, which chemical shift differences between Rho and it D51E mutant are larger than 0.1 ppm, are connected with the arrow.

E51Hα and between E51Hγ and E51Hβ in D51E mutant were observed (Supporting Information Figure S2). These results indicate that there is no difference in the overall structures of Rho and its D51E mutant. The RGD motif, the binding site for integrin, lies in a nine-residue loop joining two strands (residues 43–45 and 55–57) of a β-sheet. The RGD/E loop extends outward from the protein core with the RGD/E sequence at its apex in a four-residue RG[D/E]M type I turn. The strip plots of ^{15}N-edited NOESY of Rho are shown in Supporting Information Figure S1. The formation of a type-I turn in the $R^{49}G[D/E]M^{52}$ motif was supported by medium NOEs between $[D/E]^{51}NH$ and $M^{52}NH$, and between $G^{50}NH$ and $[D/E]^{51}NH$, as well as the weak NOEs between $P^{48}\gamma H$ and $D^{51}NH$, $R^{49}NH$ and $M^{52}NH$, and $G^{50}\alpha H$ and $M^{52}NH$. In contrast to other disintegrins determined by NMR, we observed three additional medium range NOEs, indicating that the conformations of the RGD motif in Rho and its D51E mutant were more constrained.

We identified an average of 14.9 restraints per residue for both proteins (Table I). 3D Structures of Rho and its D51E mutant were calculated using the experimentally derived restraints of 1014 and 1012, respectively. The 20 best structures of Rho and its D51E mutant from 50 initial structures are shown in Figures 4(A,B). The backbone RMSD values of Rho and its D51E mutant were 1.08 ± 0.17 Å and 1.08 ± 0.23 Å, respectively. The backbone RMSD values of Rho and D51E mutant for three β-sheet regions (13–14, 20–21, 33–34, 37–38, 43–45, and 55–57) were 0.43 ± 0.14 Å and 0.42 ± 0.14 Å, respectively. Based on the Ramachandran analysis, all dihedral angles of Rho and its D51E mutant were in the allowed region. A summary of the restraints and structural statistics is

presented in Table I. A ribbon representation of the average structure of Rho is shown in Figure 2(C). Overall, the tertiary fold of Rho and its D51E mutant has an elongated and asymmetric shape and consists of three two-stranded antiparallel β-sheets with many tight turns and loops. Their structures are organized into two constrained sub-domains, residues 1–26 and 27–68. NOE-contacts indicated that two domains were connected by the interactions between the sidechains of Q26, the phenyl ring of F38, and the main chain of Q60-S61-A62-D63. The R49-G50-D51-M52 sequence, which adopts a type-I turn structure, is located at the apex of a nine-residue loop connecting the two strands of a distorted β-sheet. NOE contacts between P48 and D54 locked the RGD loop to present the RGD motif, maintenance of which may be important to keep the RGD site in a stretched form between two β-strands. Therefore, the R49 and D51 sidechains in the loop do not interact, but point away from each other in almost opposite directions.

Comparison with 3D structures of other disintegrins

Six 3D structures of monomeric disintegrins, including kistrin, echistatin, flavoridin, albolabrin, salmosin, and trimestatin, were determined using NMR spectroscopy and X-ray crystallography.[15–20] Analysis of these structure showed that they have similar 3D structures. The 3D structures of kistrin and trimestatin were selected to compare with our structure because Rho has the same patterns of disulfide bonds and shares 100% and 75% sequence identity with kistrin and trimestatin, respectively.[15,17] We selected the structures from 20 Rho and

Table I
Summary of Structural Restraints and Statistics for Rho and its D51E Mutant

Restraints used in the structure calculation	Rho	D51E Mutant
Distance and dihedral angle restraints		
Intraresidue	141	144
Sequential	104	104
Medium range	330	327
Long range	375	373
Hydrogen bonds	9	9
Dihedral angles	55	55
Total	1014	1012
Energy statistics		
X-PLOR energy (kcal mol^{-1})		
E_{NOE}	17.85 ± 2.78	11.63 ± 2.89
E_{vdw}	13.96 ± 3.22	8.73 ± 2.79
Geometric statistics		
Deviations from idealized geometry		
All backbone atoms (Å)	1.08 ± 0.17	1.08 ± 0.23
Backbone atoms (13–14, 20–21, 33–34, 37–38, 43–45, and 55–57) (Å)	0.43 ± 0.14	0.42 ± 0.14
All heavy atoms (Å)	1.70 ± 0.28	1.67 ± 0.20
Heavy atoms (13–14, 20–21, 33–34, 37–38, 43–45, and 55–57) (Å)	0.91 ± 0.17	0.98 ± 0.15
Ramachandran analysis		
Most favored regions (%)	75.6	76.7
Additionally allowed regions (%)	22.7	21.9
Generously allowed regions (%)	1.7	1.5
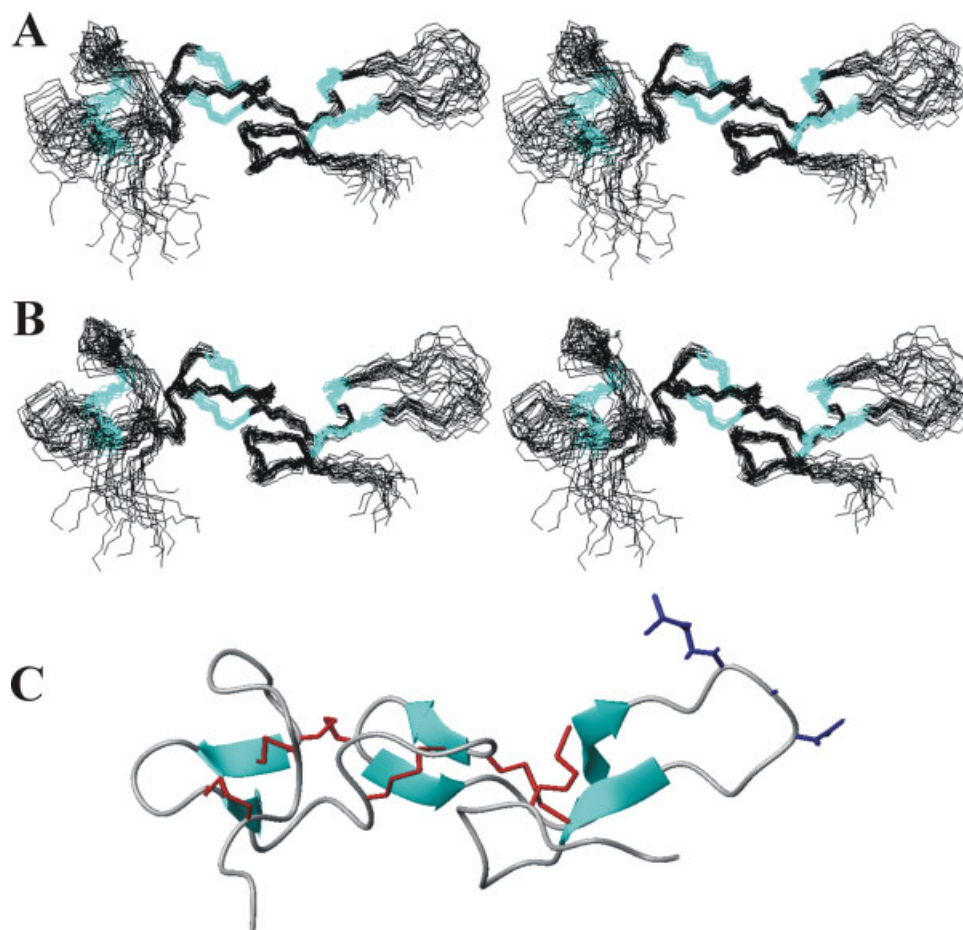
Figure 2

Structure of Rho and its D51E Mutant. Stereoview of 20 lowest-energy NMR structures of Rho (**A**) and its D51E mutant (**B**). Ribbon representation of the averaged structure of Rho (**C**). The β-strands, disulfide bonds, and the sidechains in the RGD motif of Rho are shown in light blue, red, and blue, respectively.

18 kistrin NMR structures, which has the lowest RMSD to their average structures, to perform superimposition. Superimpositions of the backbone atoms of the Rho and kistrin NMR structures and trimestatin X-ray structure resulted in the RMSD value of 1.61 Å for Rho and kistrin, and 1.79 Å for Rho and trimestatin (see Fig. 3). Structural analysis showed that 3D structures of disintegrins have similar folds, and that their major structural differences were the loop and N- and C-terminal regions. Although the residues flanking the RGD motif of disintegrins are different, they use the same conformation to present the RGD motif (see Fig. 3).

### Structural difference between Rho and its D51E mutant

3D structures of Rho and its D51E mutant have the same tertiary fold (see Fig. 2). The orientation of the RG[D/E] motif is not well defined because of few NOEs (Supporting Information Figure S2). In contrast to the RGD motif, the residues adjacent to the RGD motif were well defined with many NOEs. To compare their loop conformations, 10 of 20 Rho and its D51E mutant structures were selected to align the nine-residue RGD loop. The RMS deviations of the nine-residue backbone atoms of Rho and its D51E mutant were 0.55 and 0.48 Å, respectively (see Fig. 4). This structural analysis suggested that their RGD loops have the same backbone conformation. The only apparent difference was the charge separation between the sidechains of positive (R49) and negative residues (D51 or E51). It is known that the distance between the anionic (D) and cationic (R) terminals is crucial for optimal binding affinity and specificity for various integrins.[7,10] Therefore, this difference may contribute their functional difference.

Dynamics difference between Rho and its D51E mutant

^{1}H-^{15}N correlated NMR spectroscopy was used to measure ^{15}N R_1, ^{15}N R_2, and ^{1}H-^{15}N NOE parameters
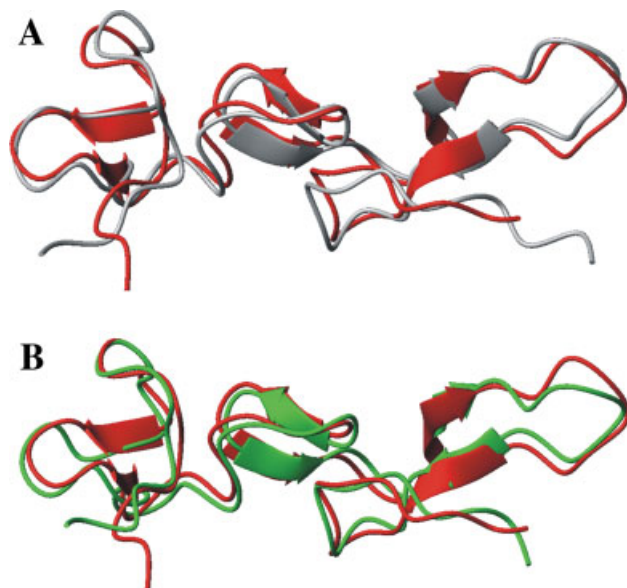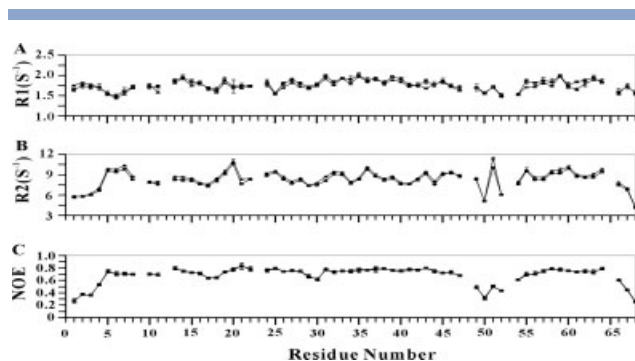
Figure 3

Superimpositions of the 3D structures of Rho (2PJF) and trimestatin (1J2L) (**A**), and Rho and kistrin (1N4Y) (**B**). Rho, trimestatin, and kistrin are shown in red, grey, and green, respectively.

for Rho and its D51E mutant. All three relaxation parameters were similar throughout the sequence (see Fig. 5). The only observable difference was found in R_2 of D51 and E51, which were 10.03 $\pm$ 0.02 and 11.37 $\pm$ 0.20 s^{-1}, respectively. The RGD loop and N- and C-terminal regions with low NOE values showed distinctive backbone flexibility which is consistent with the NMR structure of Rho. The square of the generalized order parameter (S^2), the effective internal correlation time (τ_e), and a conformational exchange broadening parameter (Rex) for each backbone amide NH vector were determined using the model-free formalism.[41] As Rho is an axially symmetric ellipsoid with the overall molecular dimension of 45 $\times$ 16 $\times$ 15 Å, the axially symmetric model was used for the analysis. Starting from the initial estimates of τ_m, D$_{//}$/D$_\perp$, θ, and ψ, we analyzed the ^{15}N relaxation data by using axially symmetric models for rotational diffusion tensor. The parameters were iteratively refined along with S2 and τ_e parameters to fit the R_1, R_2, and NOE data according to model selection procedure described by Mandel et al..[40] The selected models for the residues of Rho and its D51E mutant were shown in supporting Information Figure S3. The optimized values of τ_m for Rho and its D51E mutant were determined to be 6.2 ns and 6.4 ns, respectively. These values were larger than those estimated from the trimmed mean R_2/R_1 ratios, which were 4.6 ns and 4.9 ns, respectively. The obtained diffusion tensors of RGD and its D51E mutant were fully asymmetric with D$_{//}$/D$_\perp$ = 1.24 and 1.25,
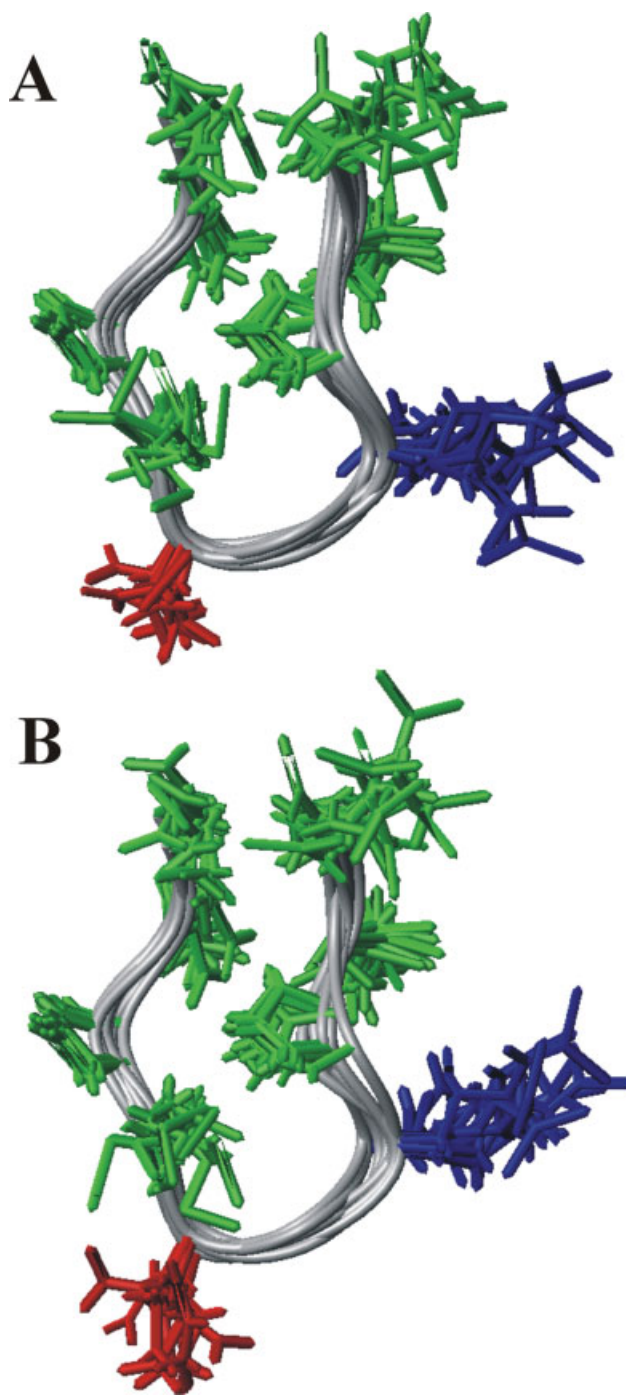
Figure 4

Structural alignments of the nine-residue RGD loop containing RIPRG[D/E]MPD sequences of Rho (**A**) and its D51E mutant (**B**). Ten of twenty Rho and its D51E mutant structures were aligned, and the RMS deviations of the nine-residue backbone atoms of Rho and its D51E mutant were 0.551 and 0.475 Å, respectively. The sidechains of R49, D51/E51, and others are shown in blue, red, and green, respectively.
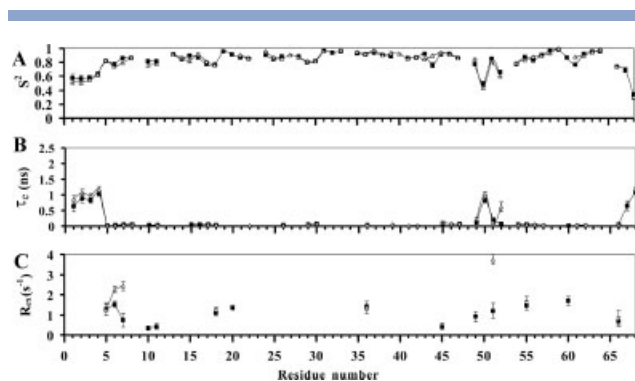
Figure 5

Comparison of the relaxation parameters of Rho (■) and its D51 mutant (△). ^{15}N R_1 with error (**A**). ^{15}N R_2 with error (**B**).^1H-^{15}N steady-state NOE with error (**C**).

Table II
Relaxation Data and Dynamic Parameters of RGD-Containing Proteins

	R_1 (s^{-1})	R_2 (s^{-1})	NOE	S^2
R49$^{WT\,a}$	1.69 ± 0.08	8.32 ± 0.13	0.48 ± 0.01	0.75 ± 0.01
R49$^{D51E\,b}$	1.70 ± 0.01	8.44 ± 0.10	0.49 ± 0.03	0.84 ± 0.01
R78$^{FN10\,c}$				0.46
R76$^{TN3\,c}$				0.86
G50$^{WT\,a}$	1.55 ± 0.02	5.09 ± 0.03	0.32 ± 0.02	0.50 ± 0.03
G50$^{D51E\,b}$	1.58 ± 0.01	5.13 ± 0.07	0.31 ± 0.02	0.43 ± 0.02
G79$^{FN10\,c}$				0.39
G77$^{TN3\,c}$				0.83
G25$^{Ech\,d}$	2.44 ± 1.27	9.06 ± 1.58	0.35 ± 0.02	0.50 ± 0.02
D51$^{WT\,a}$	1.72 ± 0.03	**10.03 ± 0.02**	0.50 ± 0.02	0.85 ± 0.01
E51$^{D51E\,b}$	1.70 ± 0.01	**11.37 ± 0.20**	0.50 ± 0.02	0.80 ± 0.01
D80$^{FN10\,c}$				0.52
D78$^{TN3\,c}$				0.77
D26$^{Ech\,d}$	2.86 ± 1.01	5.88 ± 1.40	0.46 ± 0.02	0.46 ± 0.02

^{a}Values in boldface represent the major difference between Rho and D51E mutant.
$_b$Rhodostomin from this study.
$_c$Rhodotomin D51E mutant from this study.
Dynamical properties of type III domain of fibronectin and Tenascin reported by Carr et al.[47]
^{d}Dynamical properties of echistatin reported by Chen et al.[45]

respectively. These results were consistent with our structural analysis that the tertiary fold of Rho and its D51E mutant had an elongated shape.

The optimized values of S^2, τ_m, and Rex for Rho and its D51E mutant are shown in Figure 6. The average S^2 values of Rho and its D51E mutants were 0.77 and 0.78, respectively. A summary of these values of the residues R49, G50, and [D/E]51 are presented in Table II, and the S^2 values of the R, G, and D residues in the RGD motif of Rho were 0.78 ± 0.01, 0.50 ± 0.03, and 0.85 ± 0.01, respectively. Similarly, the S^2 values of the R, G, and E residues of D51E mutant were 0.84 ± 0.01, 0.43 ± 0.01, and 0.80 ± 0.01, respectively. The S^2 values of the R and D residues are close to the average S^2 value of Rho, suggesting the rigidity of these residues. In contrast, the residue G50 has high flexibility, which may

Figure 6

Comparison of model-free parameters of Rho (■) and its D51 mutant (△). Generalized order parameters S^2, τ_e, and R_{ex}. Gaps indicate the proline residues, and the β-sheet secondary structure is shown. Comparison of internal timescale parameters, τ_e, of Rho and its D51E Mutant (B). Only some fitting models resulted in a τ_e term. Comparison of the conformational exchange terms, R_{ex}, for Rho and its D51E mutant (C). Only some fitting models resulted in an R_{ex} term.

facilitate equilibrium-binding of the RGD motif to a range of different contacts. Compared with the rest of the Rho backbone, only the S^2 value of the residue H68 was lower than that of G50. Overall, the residues of N- and C- terminal regions and the RGD loop exhibited extensive flexibility on fast motion on the ps/ns time scale.

Comparison with the dynamical properties of RGD-containing proteins

Backbone dynamics of many RGD-containing peptides and proteins, including echistatin, fibronectin, tenascin, and decorsin, were determined using NMR spectroscopy.[45–48] Analyses of the results indicate that the dynamic properties of the RGD motif affect their specificity and binding affinity to integrins. For example, the flexibility of the RGD loop in fibronectin and echistatin supports their recognition to diverse integrins.[46,47] In contrast, the more rigid RGD loop in tenascin and decorsin reflects their specificity for particular integrins.[48,49] In the present study, we found that only G50 and M52 residues in the RGD loop had S^2 values lower than the average of 0.83. The S^2 values of the G50 residue in the RGD motif of Rho and D51 E mutant were 0.50 and 0.42, which were similar to those of echistatin and fibronectin with the values of 0.50 and 0.39, respectively (Table II). In contrast to fibronectin and echistatin, but similar to tenascin and decorsin, the R49 and D51 residues in the RGD motif of Rho, with S^2 values of 0.78 and 0.85, exhibited rigidity as similar to that of the other regions. This result suggests that the more rigid R and D residues of Rho may exist in a conformation that favors binding to β1- and β3-associated integrins.

Interaction difference in the docking models of integrin αvβ3-Rho and -D51E mutant complexes

The docking of Rho and its D51E mutant into integrin αvβ3 was used to identify their integrin-interacting residues. The models of these integrin αvβ3 complexes were built using HADDOCK 1.3 software.[42] The distance and hydrogen bond restraints were derived from X-ray structure of integrin αvβ3 complexed with a cyclic RGD pentapeptide (PDB code 1L5G), and the restraints between the R, G, and D residues and integrin αvβ3 were 34, 10, and 40 contacts, respectively (Table III).[43] Eight key interactions were found between integrin and the R and D residues, respectively. Specifically, the R residue of the cyclic peptide forms a bidentate salt-bridge hydrogen bond with the D218 residue and a hydrogen bond with the D150 residue of αv subunit. The carboxylate oxygen of the D residue of the cyclic peptide contacts a Mn^{2+} ion and forms hydrogen bonds with the residues S121 and S123 of β3 subunit. The other carboxyl oxygen of the D residue of the cyclic peptide forms hydrogen bonds with the residues Y122 and N215 of β3 subunit, and the backbone amide of the D residue forms hydrogen bond with the R216 residue of β3 subuint [Fig. 7(A)]. Using these restraints, we performed the dockings of Rho to integrin αvβ3 in the presence and absence of six restraints between the backbone atoms of the D51 residue and the atoms of integrin. The analysis showed that the docking of Rho into integrin αvβ3 with and without six D51 backbone atom interactions resulted in the same numbers of contacts (Table III). The key contacts included seven hydrogen bonds and two salt bridges between the R and D residues of the RGD motif and integrin, and the total numbers of interactions between the backbone atoms of the D51 residue and the atoms of integrin were 9.3 ± 2.3 and 9.3 ± 1.5, respectively (Table III). In particular, we found that the backbone carbonyl group of the D residue also forms hydrogen bond with R214 [Fig. 7(B)]. In contrast, the docking of D51E mutant into integrin αvβ3 without six E51 backbone atom interactions resulted in 4.8 ± 2.1 contacts, and the interactions between backbone amide and carbonyl groups of E51 and the atoms of β3 subunit were absent [Fig. 7(C)]. Thus, the hydrogen bonds between the backbone amide and carbonyl groups of the E51 residue of the D51E mutant and the residues R214 and R216 of integrin β3 subunit were not formed due to the longer sidechain of E51 [Fig. 7(D)].

DISCUSSION

Many reports have shown that the conserved R and D residues of disintegrins play the most important role in interacting with RGD-binding integrins.[6–11] In the present study we expressed Rho and its D51E mutant in *P. pastoris* to study the role of the D residue in function, structure, and dynamics of RGD-containing disintegrins. We found that, compared with the inhibitory activity of wild-type Rho, its D51E mutant inhibited platelet aggregation with a K_I of 49 μM, a 628-fold decrease in activity. This is consistent with previous reports that conservative D to E substitution on RGD-containing proteins and peptides caused a significant decrease in their activity in binding to integrins.[23,25,47,50] NMR analysis of Rho and its D51E mutant showed that they have the same tertiary fold with two minor differences in their backbone dynamics and 3D structures. Interestingly, the docking of Rho into integrin αvβ3 showed that backbone amide and carbonyl groups of the D51 residue of Rho were formed hydrogen bonds with integrin, and two hydrogen bonds were absent in the D51E mutant-integrin complex [Fig. 7(D)]. This study suggests that hydrogen bonds between both the sidechain and backbone of the D residue of RGD-containing ligands and integrin β3 subunit are important for their binding.

The importance of the interactions between the sidechain and backbone of the D residue of RGD-containing ligands and integrin αvβ3 is consistent with the crystal structure of the integrin αIIbβ3 in complex with the cyclic peptide eptifibatide (PDB code 1TY6). The peptide also made extensive contacts with αIIb and β3 subunits, and the number of residue contacts between the homoar-

Table III
Summary of the Interactions Between Protein and Integrin

Protein	Residue		Numbers of interaction	
			Integrin αv	Integrin β3
cRGDfV[a]	R	Backbone	3	
		Sidechain	31	
	G	Backbone		10
		Sidechain		
	D	Backbone		6[b] (0[c])
		Sidechain		34
Rho[b]	R49	Backbone	3.9 ± 1.2	
		Sidechain	34.2 ± 3.3	
	G50	Backbone		10.4 ± 1.2
		Sidechain		0.9 ± 1.3
	D51	Backbone		9.3 ± 1.5
		Sidechain		46.6 ± 1.8
Rho[c]	R49	Backbone	2.5 ± 1.8	
		Sidechain	33.5 ± 2.8	
	G50	Backbone		10.9 ± 1.6
		Sidechain		0.5 ± 1.1
	D51	Backbone		**9.3 ± 2.3**
		Sidechain		42.5 ± 2.3
D51E Mutant[c]	R49	Backbone	4.1 ± 1.6	
		Sidechain	35.2 ± 3.3	
	G50	Backbone		2.8 ± 1.4
		Sidechain		9.4 ± 2.6
	E51	Backbone		**4.8 ± 2.1**
		Sidechain		47.3 ± 2.9

[a]Numbers of interaction restraints were found from X-ray structure of integrin αvβ3 complexed with a cyclic RGD pentapeptide (PDB code 1L5G) using imoltalk.
[b]Docking models including the restraints with six backbone interactions.
[c]Docking models including the restraints without six backbone interactions.
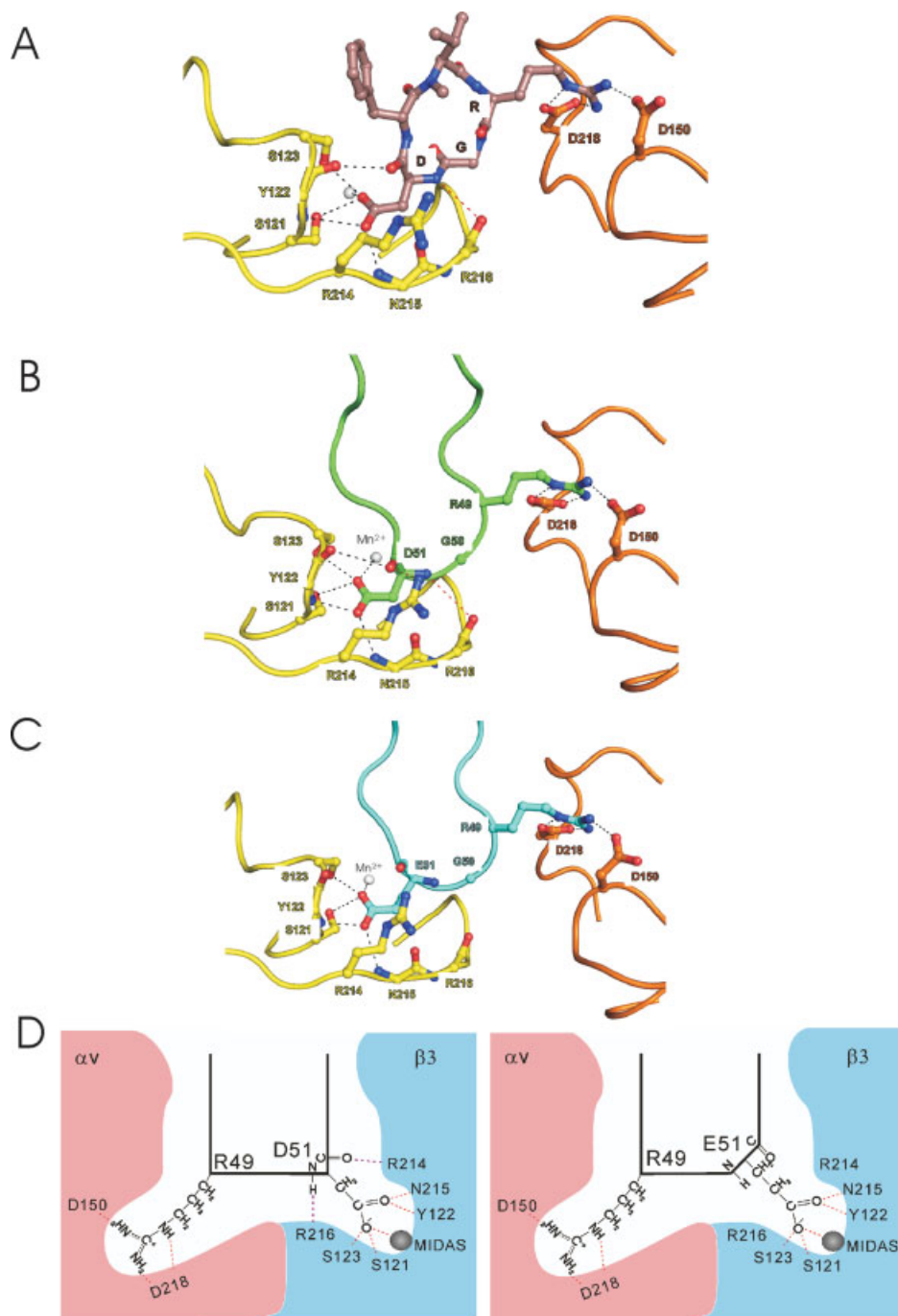
Figure 7

The interactions between integrin αvβ3 and its ligands. Only the contact surface between the RGD/E motif and integrin αvβ3 is shown, and the αv and β3 subunits are shown in yellow and orange, respectively. The interacting residues are shown in the ball-and-stick representation, and hydrogen bonds are displayed by broken lines. The β3 MIDAS Mn²⁺ ion is depicted as a gray sphere. Detailed interactions between integrin αvβ3 and the cyclic pentapeptide RGDf-N(Me)V (**A**). Detailed interactions between integrin αvβ3 and Rho (**B**). Detailed interactions between integrin αvβ3 and Rho D51E mutant (**C**). Schematic diagram showing the interaction difference between the docking models of integrin αvβ3-Rho and -D51 mutant complexes (**D**).

ginine (Hrg), G, and D residues and integrin αIIbβ3 were 13, 3, and 18, respectively.[51] The main difference in ligand interactions between integrin αvβ3 and αIIbβ3 complexes was van der Waals contacts. In contrast, eight key interactions, including six hydrogen bonds and two salt bridge interactions, are the same. The analysis

showed that not only the sidechain but also the backbone atoms of the D residue of eptifibatide were extensively interacted with integrin. The backbone amide group of the D residue formed hydrogen bond with the R216 residue, and the backbone carbonyl group also contacted with the $C\beta$ and $C\delta_2$ carbon atoms of the Tyr122 residue. Therefore, we hypothesized that the E residue containing additional $C\gamma$ carbon atom may hamper the binding of its backbone amide and carbonyl groups to integrin. This hypothesis is consistent with previous reports that the key feature of RGD-associated integrin antagonists contains an anionic carboxy-terminal (CO_2^-) adjacent to the amide and/or carbonyl groups, which may be important for interacting with integrins.[52,53]

The backbone dynamics of Rho and its D51E mutant, which we studied using ^{15}N nuclear spin relaxation provides the first complete dynamics study of the medium-sized disintegrins. We found that R and D residues of the RGD motif in Rho are as rigid as regular elements of secondary structures. As indicated by the lower order parameters shown in Figure 7, the N- and C-terminal regions, as well as the G50 and M52 residues of the RGD loop in Rho, were mobile. The conformational freedom of the residues in the RGD loop of Rho is consistent with reports that the flexibility and solvent exposure of this loop may be responsible for fast recognition and fitting to integrin receptors.[54,55] In contrast, the order parameter of the R and D residues of the RGD motif in Rho is are similar to those of tenascin, suggesting that the rigidity of the residues of R and D in Rho results in its specific binding to $\beta1$- and $\beta3$-associated integrins with greater affinity.[47–49] The only observable difference between Rho and its D51E mutant was found in the R_2 of D51 and E51 (10.03 ± 0.02 and 11.37 ± 0.20 s^{-1}). It is possible that this difference may also play a role in their interaction with integrins.

Structural analyses of Rho and its D51E mutant showed that they had the same tertiary fold and identical backbone conformations in the RGD/E motif. The only difference is additional $C\gamma$ atom of E51, resulting in a charge separation of the sidechains between R49 and E51 than between R49 and D51. The average distances between $C\zeta$-to-$C\gamma$ of the R and D residues of Rho and between $C\zeta$-to-$C\delta$ of the R and E residues of D51E mutant were 11.41 ± 1.99 and 13.17 ± 1.52 Å, respectively. Although the difference between and Rho and its D51E mutant was 1.76 Å, the spread of values is large and has a deviation of 1.99 Å. The analysis suggested that this difference, but not backbone conformation, may also play a role for the activity difference between Rho and its D51E mutant. This speculation is consistent with previous reports that the key feature of integrin $\alpha IIb\beta3$ antagonists is the presence of an anionic carboxy-terminal (CO_2^-) separated by a spatial chemical moiety and a certain distance from the cationic basic amino-terminal of benzamidine, piperidine, and guanidine.[47,50] We can-

not, however, exclude that the interaction with integrin stabilizes a particular conformation of D and E residues in Rho that cannot be adapted by the D51E mutant.

In conclusion, this is the first comparison of the functional, structural, and dynamic differences between RGD-containing protein and its inactive RGE mutant. Although Rho and its D51E mutant exhibited a 628-fold difference in activity in the inhibition of platelet aggregation, we only found two minor differences between their backbone dynamics and 3D structures. The R_2 value of E51 is 13% higher than that of the D51 residue and the charge separation between the sidechains of positive (R49) and negative (E51) residues is 1.76 Å larger in the inactive D51E mutant than in Rho. Based on the docking structures of integrin $\alpha v\beta3$ in complex with Rho and its D51E mutant, the backbone amide and carbonyl groups of the D51 residue of Rho were formed hydrogen bonds with the subunit $\beta3$ residues R216 and R214, respectively. In contrast, these interactions were absent in the D51E mutant-integrin complex. The occurrence of the interactions between both the sidechain and backbone of the D residue of RGD-containing ligands and integrin highlight the importance of the conserved D residue in the RGD motif. Our findings provide new insights into the interactions of integrins with their RGD-ligands in solution. They also provide important structural and dynamic information for the design of more potent RGD mimetics and serve as a basis for exploring the structure and functional relationships of R GD-binding integrins and their ligands.

REFERENCES

1. Vale R, Kreis T. Guidebook to the extracellular matrix, anchor and adhesion proteins. Oxford, New York: Oxford University Press; 1999.
2. Humphries MJ, McEwan PA, Barton SJ, Buckley PA, Bella J, Mould AP. Integrin structure: heady advances in ligand binding, but activation still makes the knees wobble. Trends Biochem Sci 2003;28:313–320.
3. Plow EF, Haas TA, Zhang L, Loftus J, Smith JW. Ligand binding to integrins. J Biol Chem 2000;275:21785–21788.
4. Xiong JP, Stehle T, Goodman SL, Arnaout MA. New insights into the structural basis of integrin activation. Blood 2003;102:1155–1159.
5. Shimaoka M, Takagi J, Springer TA. Conformational regulation of integrin structure and function. Annu Rev Biophys Biomol Struct 2002;31:485–516.
6. Ruoslahti E. RGD and other recognition sequences for integrins. Annu Rev Cell Dev Biol 1996;12:697–715.
7. McLane MA, Sanchez EE, Wong A, Paquette-Straub C, Perez JC. Disintegrins Curr Drug Targets Cardiovasc Haematol Disord 4:327–355, 2004.
8. Mans BJ, Louw AI, Neitz AW. Savignygrin, a platelet aggregation inhibitor from the soft tick Ornithodoros savignyi, presents the RGD integrin recognition motif on the Kunitz-BPTI fold. J Biol Chem 2002;277:21371–21378.
9. Chen CY, Luo SC, Kuo CF, Lin YS, Wu JJ, Lin MT, Liu CC, Jeng WY, Chuang WJ. Maturation processing and characterization of streptopain. J Biol Chem 2003;278:17336–17343.

10. Shiu JH, Chen CY, Chang LS, Chen YC, Chen YC, Lo YH, Liu YC, Chuang WJ. Solution structure of gamma-bungarotoxin: the functional significance of amino acid residues flanking the RGD motif in integrin binding. Proteins 2004;57:839–849.

11. Wang FZ, Akula SM, Sharma-Walia N, Zeng L, Chandran B. Human herpesvirus 8 envelope glycoprotein B mediates cell adhesion via its RGD sequence. J Virol 2003;77:3131–3147.

12. McLane MA, Marcinkiewicz C, Vijay-Kumar S, Wierzbicka-Patynowski I, Niewiarowski S. Viper venom disintegrins and related molecules. Proc Soc Exp Biol Med 1998;219:109–119.

13. Niewiarowski S, McLane MA, Kloczewiak M, Stewart GJ. Disintegrins and other naturally occurring antagonists of platelet fibrinogen receptors. Semin Hematol 1994;31:289–300.

14. Blobel CP, White JM. Structure, function and evolutionary relationship of proteins containing a disintegrin domain. Curr Opin Cell Biol 1992;4:760–765.

15. Adler M, Lazarus RA, Dennis MS, Wagner G. Solution structure of kistrin, a potent platelet aggregation inhibitor and GP IIb-IIIa antagonist. Science 1991;253:445–448.

16. Saudek V, Atkinson RA, Pelton JT. Three-dimensional structure of echistatin, the smallest active RGD protein. Biochemistry 1991;30:7369–7372.

17. Senn H, Klaus W. The nuclear magnetic resonance solution structure of flavoridin, an antagonist of the platelet GP IIb-IIIa receptor. J Mol Biol 1993;232:907–925.

18. Smith KJ, Jaseja M, Lu X, Williams JA, Hyde EI, Trayer IP. Three-dimensional structure of the RGD-containing snake toxin albolabrin in solution, based on 1H NMR spectroscopy and simulated annealing calculations. Int J Pept Protein Res 1996;48:220–228.

19. Fujii Y, Okuda D, Fujimoto Z, Horii K, Morita T, Mizuno H. Crystal structure of trimestatin, a disintegrin containing a cell adhesion recognition motif RGD. J Mol Biol 2003;332:1115–1122.

20. Shin J, Hong SY, Chung K, Kang I, Jang Y, Kim DS, Lee W. Solution structure of a novel disintegrin, salmosin, from Agkistrondon halys venom. Biochemistry 2003;42:14408–14415.

21. Marcinkiewicz C, Vijay-Kumar S, McLane MA, Niewiarowski S. Significance of RGD loop and C-terminal domain of echistatin for recognition of αIIb β3 and α(v) β3 integrins and expression of ligand-induced binding site. Blood 1997;90:1565–1575.

22. McLane MA, Vijay-Kumar S, Marcinkiewicz C, Calvete JJ, Niewiarowski S. Importance of the structure of the RGD-containing loop in the disintegrins echistatin and eristostatin for recognition of αIIb β3 and αv β3 integrins. FEBS Lett 1996;391:139–143.

23. Dennis MS, Carter P, Lazarus RA. Binding interactions of kistrin with platelet glycoprotein IIb-IIIa: analysis by site-directed mutagenesis. Proteins 1993;15:312–321.

24. Cherny RC, Honan MA, Thiagarajan P. Site-directed mutagenesis of the arginine-glycine-aspartic acid in vitronectin abolishes cell adhesion. J Biol Chem 1993;268:9725–9729.

25. Johnson WC, Jr, Pagano TG, Basson CT, Madri JA, Gooley P, Armitage IM. Biologically active Arg-Gly-Asp oligopeptides assume a type II β-turn in solution. Biochemistry 1993;32:268–273.

26. Huang TF, Sheu JR, Teng CM, Chen SW, Liu CS. Triflavin, an antiplatelet Arg-Gly-Asp-containing peptide, is a specific antagonist of platelet membrane glycoprotein IIb-IIIa complex. J Biochem 1991;109:328–334.

27. Guo RT, Chou LJ, Chen YC, Chen CY, Pari K, Jen CJ, Lo SJ, Huang SL, Lee CY, Chang TW, Chuang WJ. Expression in Pichia pastoris and characterization by circular dichroism and NMR of rhodostomin. Proteins 2001;43:499–508.

28. Chen CY, Cheng CH, Chen YC, Lee JC, Chou SH, Huang W, Chuang WJ. Preparation of amino-acid-type selective isotope labeling of protein expressed in Pichia pastoris. Proteins 2006;62:279–287.

29. Aiyar A, Xiang Y, Leis J. Site-directed mutagenesis using overlap extension PCR. Methods Mol Biol 1996;57:177–191.

30. Schagger H, von Jagow G. Tricine-sodium dodecyl sulfate-polyacrylamide gel electrophoresis for the separation of proteins in the range from 1 to 100 kDa. Anal Biochem 1987;166:368–379.

31. Wuthrich K. NMR of proteins and nucleic acids. New York: John Wiley & Sons; 1986.

32. Kay LE, Marion D, Bax A. Practical aspects of 3d heteronuclear Nmr of proteins. J Magn Reson 1989;84:72–84.

33. Brunger AT. X-PLOR : version 3.1: a system for x-ray crystallography and NMR. New Haven: Yale University Press; 1992.

34. Nilges M, Clore GM, Gronenborn AM. Determination of three-dimensional structures of proteins from interproton distance data by dynamical simulated annealing from a random array of atoms. Circumventing problems associated with folding. FEBS Lett 1988;239:129–136.

35. Wagner G, Braun W, Havel TF, Schaumann T, Go N, Wuthrich K. Protein structures in solution by nuclear magnetic resonance and distance geometry. The polypeptide fold of the basic pancreatic trypsin inhibitor determined using two different algorithms, DISGEO and DISMAN. J Mol Biol 1987;196:611–639.

36. Koradi R, Billeter M, Wuthrich K. MOLMOL: a program for display and analysis of macromolecular structures. J Mol Graph 1996;14:51–55, 29–32.

37. Kordel J, Skelton NJ, Akke M, Palmer AG, III, Chazin WJ. Backbone dynamics of calcium-loaded calbindin D9k studied by two-dimensional proton-detected 15N NMR spectroscopy. Biochemistry 1992;31:4856–4866.

38. Cole R, Loria JP. FAST-Modelfree: a program for rapid automated analysis of solution NMR spin-relaxation data. J Biomol NMR 2003;26:203–213.

39. Lipari G, Szabo A. Model-free approach to the interpretation of nuclear magnetic resonance relaxation in macromolecules. I. Theory and range of validity. J Am Chem Soc 1982;104:4546–4559.

40. Mandel AM, Akke M, Palmer AG, III. Backbone dynamics of Escherichia coli ribonuclease HI: correlations with structure and function in an active enzyme. J Mol Biol 1995;246:144–163.

41. Lee LK, Rance M, Chazin WJ, Palmer AG, III. Rotational diffusion anisotropy of proteins from simultaneous analysis of 15N and 13C nuclear spin relaxation. J Biomol NMR 1997;9:287–298.

42. Dominguez C, Boelens R, Bonvin AM. HADDOCK: a protein-protein docking approach based on biochemical or biophysical information. J Am Chem Soc 2003;125:1731–1737.

43. Xiong JP, Stehle T, Zhang R, Joachimiak A, Frech M, Goodman SL, Arnaout MA. Crystal structure of the extracellular segment of integrin alpha Vβ3 in complex with an Arg-Gly-Asp ligand. Science 2002;296:151–155.

44. Diemand AV, Scheib H. iMolTalk: an interactive, internet-based protein structure analysis server. Nucleic Acids Res 2004;32 (Web Server issue):W512–W516.

45. Chen Y, Suri AK, Kominos D, Sanyal G, Naylor AM, Pitzenberger SM, Garsky VM, Levy RM, Baum J. Three-dimensional structure of echistatin and dynamics of the active site. J Biomol NMR 1994;4:307–324.

46. Monleon D, Esteve V, Kovacs H, Calvete JJ, Celda B. Conformation and concerted dynamics of the integrin-binding site and the C-terminal region of echistatin revealed by homonuclear NMR. Biochem J 2005;387:57–66.

47. Carr PA, Erickson HP, Palmer AG, III. Backbone dynamics of homologous fibronectin type III cell adhesion domains from fibronectin and tenascin. Structure 1997;5:949–959.

48. Krezel AM, Ulmer JS, Wagner G, Lazarus RA. Recombinant decorsin: dynamics of the RGD recognition site. Protein Sci 2000;9:1428–1438.

49. Pankov R, Yamada KM. Fibronectin at a glance. J Cell Sci 2002;115:3861–3863.

50. Pfaff M, McLane MA, Beviglia L, Niewiarowski S, Timpl R. Comparison of disintegrins with limited variation in the RGD loop in their binding to purified integrins α IIb β 3, α V β 3 and α 5 β 1 and in cell adhesion inhibition. Cell Adhes Commun 1994;2:491–501.

51. Xiao T, Takagi J, Coller BS, Wang JH, Springer TA. Structural basis for allostery in integrins and binding to fibrinogen-mimetic therapeutics. Nature 2004;432:59–67.

52. Gottschalk KE, Kessler H. The structures of integrins and integrin-ligand complexes: implications for drug design and signal transduction. Angew Chem Int Ed Engl 2002;41:3767–3774.

53. Meyer A, Auernheimer J, Modlinger A, Kessler H. Targeting RGD recognizing integrins: drug development, biomaterial research, tumor imaging and targeting. Curr Pharm Des 2006;12:2723–2747.

54. Copie V, Tomita Y, Akiyama SK, Aota S, Yamada KM, Venable RM, Pastor RW, Krueger S, Torchia DA. Solution structure and dynamics of linked cell attachment modules of mouse fibronectin containing the RGD and synergy regions: comparison with the human fibronectin crystal structure. J Mol Biol 1998;277: 663–682.

55. Main AL, Harvey TS, Baron M, Boyd J, Campbell ID. The three-dimensional structure of the tenth type III module of fibronectin: an insight into RGD-mediated interactions. Cell 1992;71: 671–678.